



# Computation of thermal fracture parameters for orthotropic functionally graded materials using $J_k$ -integral

Serkan Dag<sup>a,\*</sup>, E. Erhan Arman<sup>a</sup>, Bora Yildirim<sup>b</sup>

<sup>a</sup> Department of Mechanical Engineering, Middle East Technical University, Ankara 06531, Turkey

<sup>b</sup> Department of Mechanical Engineering, Hacettepe University, Ankara 06800, Turkey

## ARTICLE INFO

### Article history:

Received 10 March 2010

Received in revised form 30 July 2010

Available online 28 September 2010

### Keywords:

Orthotropic functionally graded materials

$J_k$ -integral

Finite element method

Thermal stresses

Stress intensity factors

## ABSTRACT

This article introduces a computational method based on the  $J_k$ -integral for mixed-mode fracture analysis of orthotropic functionally graded materials (FGMs) that are subjected to thermal stresses. The generalized definition of the  $J_k$ -integral is recast into a domain independent form composed of line and area integrals by utilizing the constitutive relations of plane orthotropic thermoelasticity. Implementation of the domain independent  $J_k$ -integral is realized through a numerical procedure developed by means of the finite element method. The outlined computational approach enables the evaluation of the modes I and II stress intensity factors, the energy release rate, and the  $T$ -stress. The developed technique is validated numerically by considering two different problems, the first of which is the problem of an embedded crack in an orthotropic FGM layer subjected to steady-state thermal stresses; and the second one is that of periodic cracks under transient thermal loading. Comparisons of the mixed-mode stress intensity factors evaluated by the  $J_k$ -integral based method to those calculated through the displacement correlation technique (DCT) and to those available in the literature point out that, the proposed form of the  $J_k$ -integral possesses the required domain independence and leads to numerical results of high accuracy. Further results are presented to illustrate the influences of the geometric and material constants on the thermal fracture parameters.

© 2010 Elsevier Ltd. All rights reserved.

## 1. Introduction

Functionally graded materials (FGMs) belong to a certain class of composite materials that possess smooth spatial variations in the volume fractions of the constituents. These variations lead to a nonhomogeneous structure and require that the physical properties be represented by continuous functions for analytical and computational purposes. FGMs have been utilized in a number of technological applications such as thermal barrier coatings (Kawasaki and Watanabe, 2002), solid oxide fuel cells (Liu et al., 2004), high performance cutting tools (Nomura et al., 1999), and biomedical materials (Watari et al., 2004). Depending on the characteristics of the processing technique employed, a functionally graded material could be orthotropic in addition to being nonhomogeneous. Functionally graded materials processed by plasma spray forming for instance have a lamellar microstructure and contain weak cleavage planes parallel to the boundaries (Sampath et al., 1995). The electron beam physical vapor deposition technique on the other hand leads to a columnar microstructure in the processed FGM with weak cleavage planes perpendicular to the bounding

surfaces (Kaysser and Ilschner, 1995). The graded materials processed by such methods are generally referred to as orthotropic FGMs. The distinctive feature of these materials from the mechanics viewpoint is that, their thermomechanical properties are both orthotropic and dependent upon the spatial coordinates (Ozturk and Erdogan, 1997; Kim and Paulino, 2004; Dag, 2006; Kim and Kc, 2008).

Various methodologies are proposed in the literature to examine the behavior of cracks located in orthotropic FGMs. One of the effective ways of conducting fracture analysis of orthotropic FGMs is to use  $J_k$ -integral in conjunction with the finite element method. In its generalized form,  $J_k$ -integral is defined as a vector at the tip of a crack (Eischen, 1987a). The  $J_k$ -integral vector has two components  $J_1$  and  $J_2$ , the former being equivalent to the  $J$ -integral of Rice (1968). Knowles and Sternberg (1972), Budiansky and Rice (1973) and Hellen and Blackburn (1975) laid out the theoretical framework of the  $J_k$ -integral within the context of mechanically-loaded homogeneous isotropic materials. Considering thermally-loaded homogeneous isotropic solids, Chen and Chen (1981) developed the formulation of the  $J_k$ -integral, and Chen and Ting (1985) introduced a  $J_k$ -integral based finite element analysis technique. Eischen (1987a) detailed an improved method for the evaluation of the second component  $J_2$  of the  $J_k$ -integral, which is applicable for homogeneous isotropic materials subjected to

\* Corresponding author. Tel.: +90 312 2102580; fax: +90 312 2102536.

E-mail address: [sdag@metu.edu.tr](mailto:sdag@metu.edu.tr) (S. Dag).

mechanical loads. For mechanically-loaded homogeneous anisotropic bodies, computational implementation of the  $J_k$ -integral is demonstrated by Chu and Hong (1990) using the finite element method and by Sollero and Aliabadi (1993) and Pan and Amadei (1996) using the boundary element method. There are a number of studies that deal with the use of the  $J_k$ -integral in mixed-mode fracture analysis of functionally graded materials. Eischen (1987b) and Kim and Paulino (2002) put forward finite element procedures employing  $J_k$ -integral for fracture analysis of graded isotropic materials subjected to mechanical loads. Work on the formulation and finite element implementation of the  $J_k$ -integral for thermal fracture analysis of isotropic FGMs is conducted by Dag (2007) and Dag and Yildirim (2009). Kim and Paulino (2003) presented a  $J_k$ -integral approach to compute the crack tip parameters for mechanically-loaded orthotropic FGMs.

The review of the technical literature, as given in the foregoing paragraph, reveals that there are no previous studies on the formulation and implementation of the  $J_k$ -integral for mixed-mode fracture analysis of orthotropic FGMs subjected to thermal stresses. In fact, the only computational studies on thermal fracture of orthotropic FGMs are those by Dag (2006), Dag et al. (2007) and Kim and Kc (2008), which respectively present methods based on  $J$ -integral, enriched finite elements, and interaction integral. The goals of the present study on the other hand are to develop the formulation of the  $J_k$ -integral for orthotropic FGMs subjected to thermal stresses, and to lay out a computational procedure for the implementation to evaluate the mixed-mode fracture parameters.

In the formulation of the  $J_k$ -integral, we consider an embedded crack lying in an orthotropic functionally graded medium that is under the effect of mixed-mode thermal loading. By using the constitutive relations of plane orthotropic thermoelasticity, the generalized definition of the  $J_k$ -integral at the tip of the embedded crack is converted to a domain independent form that comprises line and area integrals. A finite elements based numerical procedure is then introduced so as to evaluate the components  $J_1$  and  $J_2$  of the  $J_k$ -integral, the modes I and II stress intensity factors (SIFs)  $K_I$  and  $K_{II}$ , and the  $T$ -stress. Developed methodology is integrated into the general purpose finite element analysis software ANSYS (1997).

Application of the proposed procedure is demonstrated by considering two different fracture mechanics problems, the first being the problem of an embedded crack in an orthotropic FGM layer subjected to steady-state thermal stresses, and the second the problem of periodic cracks under the effect of transient thermal loading. The developed method is validated by comparing the results generated by means of the  $J_k$ -integral to those computed by the displacement correlation technique (DCT) in the case of the embedded crack problem, and to those given by Dag et al. (2007) in the case of the periodic cracking problem. The comparisons indicate that, the derived  $J_k$ -integral form is domain independent, and that the  $J_k$ -integral based finite element procedure yields numerical results of high accuracy. The results presented for the embedded crack problem also illustrate the effects of geometric and material constants upon the modes I and II stress intensity factors, the energy release rate, and the  $T$ -stress.

## 2. $J_k$ -integral for thermally-loaded orthotropic functionally graded materials

We consider an embedded crack in an orthotropic functionally graded medium that is assumed to be subjected to thermal stresses in the development of the  $J_k$ -integral. The problem geometry is depicted in Fig. 1.  $x_1$  and  $x_2$  axes, which are the principal axes of orthotropy, constitute a local coordinate system whose origin  $O$  is located at the crack tip. The linear elastic medium is in a state of either plane stress or plane strain. In the case of plane stress,

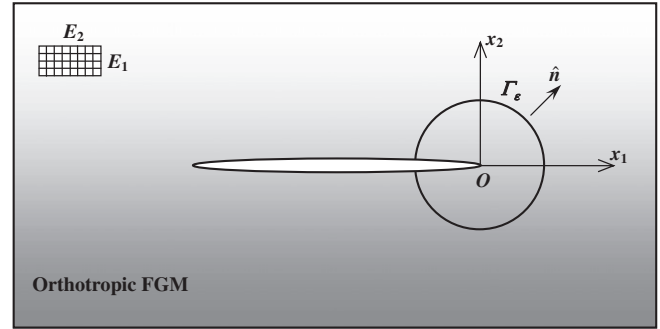


Fig. 1. An embedded crack in an orthotropic functionally graded medium.

the relations between the total strains  $\varepsilon_{ij}$  and the stresses  $\sigma_{ij}$  can be expressed in the following form:

$$\begin{bmatrix} \varepsilon_{11} \\ \varepsilon_{22} \\ 2\varepsilon_{12} \end{bmatrix} = \begin{bmatrix} 1/E_1 & -\nu_{12}/E_1 & 0 \\ -\nu_{12}/E_1 & 1/E_2 & 0 \\ 0 & 0 & 1/G_{12} \end{bmatrix} \begin{bmatrix} \sigma_{11} \\ \sigma_{22} \\ \sigma_{12} \end{bmatrix} + \begin{bmatrix} \alpha_1 \Delta T \\ \alpha_2 \Delta T \\ 0 \end{bmatrix}. \quad (1)$$

For plane strain, the constitutive relations are given by

$$\begin{bmatrix} \varepsilon_{11} \\ \varepsilon_{22} \\ 2\varepsilon_{12} \end{bmatrix} = \begin{bmatrix} (1 - \nu_{31}\nu_{13})/E_1 & -(\nu_{12} + \nu_{13}\nu_{32})/E_1 & 0 \\ -(\nu_{12} + \nu_{13}\nu_{32})/E_2 & (1 - \nu_{23}\nu_{32})/E_2 & 0 \\ 0 & 0 & 1/G_{12} \end{bmatrix} \begin{bmatrix} \sigma_{11} \\ \sigma_{22} \\ \sigma_{12} \end{bmatrix} + \begin{bmatrix} (\nu_{31}\alpha_3 + \alpha_1)\Delta T \\ (\nu_{32}\alpha_3 + \alpha_2)\Delta T \\ 0 \end{bmatrix}. \quad (2)$$

In Eqs. (1) and (2),  $E_i$ ,  $\nu_{ij}$ ,  $G_{12}$ , and  $\alpha_i$  respectively stand for the elastic modulus, the Poisson's ratio, the shear modulus, and the coefficient of thermal expansion.  $\Delta T$  is temperature difference; and equals to  $T - T_0$ ,  $T$  being the temperature of the point under consideration and  $T_0$  the reference temperature. The properties of orthotropic materials are related as

$$\frac{\nu_{12}}{E_1} = \frac{\nu_{21}}{E_2}, \quad \frac{\nu_{13}}{E_1} = \frac{\nu_{31}}{E_3}, \quad \frac{\nu_{23}}{E_2} = \frac{\nu_{32}}{E_3}. \quad (3)$$

Referring to Fig. 1, the generalized definition of the  $J_k$ -integral at the crack tip  $O$  can be written in the following way (Eischen, 1987a):

$$J_k = \lim_{\Gamma_\varepsilon \rightarrow 0} \left\{ \int_{\Gamma_\varepsilon} (Wn_k - \sigma_{ij}n_j u_{i,k}) ds \right\}, \quad (i, j, k = 1, 2), \quad (4)$$

where  $\Gamma_\varepsilon$  is an open curve whose end points are on the lower and upper crack surfaces,  $s$  is the arc-length,  $n_j$  is the unit normal vector,  $W$  is the mechanical strain energy density function,  $u_i$  represents the displacement vector, and a comma stands for partial differentiation, i.e.  $(\cdot)_{,k} \equiv \partial(\cdot)/\partial x_k$ . Note that the first component of the  $J_k$ -integral, i.e.  $J_1$ , is equivalent to the energy release rate. The mechanical strain energy density function  $W$  is expressed as

$$W = \begin{cases} \frac{1}{2} \sigma_{ij} \varepsilon_{ij}^m, & (i, j = 1, 2) \text{ for plane stress,} \\ \frac{1}{2} \sigma_{ij} \varepsilon_{ij}^m + \frac{1}{2} \sigma_{33} \varepsilon_{33}^m, & (i, j = 1, 2) \text{ for plane strain.} \end{cases} \quad (5)$$

The mechanical strains in Eq. (5) are

$$\begin{aligned} \varepsilon_{11}^m &= \varepsilon_{11} - \alpha_1 \Delta T, & \varepsilon_{12}^m &= \varepsilon_{12}, & \varepsilon_{21}^m &= \varepsilon_{21}, \\ \varepsilon_{22}^m &= \varepsilon_{22} - \alpha_2 \Delta T, & \varepsilon_{33}^m &= -\alpha_3 \Delta T. \end{aligned} \quad (6)$$

The  $\varepsilon_{33}^m$  expression given above is valid only for the case of plane strain since the total strain  $\varepsilon_{33}$  is zero for plane strain and in general nonzero for plane stress. However,  $\varepsilon_{33}^m$  is not required in the computation of  $W$  for the case of plane stress as can be seen from Eq. (5). This is due to the fact that  $\sigma_{33}$  is zero for plane stress. The explicit

expressions of  $W$  in terms of the material parameters, the total strains, and the temperature difference can be derived by using Eqs. (1), (2), (5) and (6). These expressions are available in the article by Dag (2006).

The  $J_k$ -integral defined by Eq. (4) is to be calculated over a vanishingly small open curve  $\Gamma_\varepsilon$ . However, this definition is not suitable to be implemented by means of finite elements. It is necessary to develop another form of  $J_k$ -integral that is defined and evaluated over finite domains. This is accomplished by making use of a formulation procedure, which is previously detailed by Dag (2007) for thermally-loaded isotropic functionally graded materials. The details of this procedure will not be reproduced here for brevity. By following this method, the separate components  $J_1$  and  $J_2$  of the  $J_k$ -integral are recast into the following domain independent forms:

$$J_1 = \int \int_A (\sigma_{ij} u_{i,1} - W \delta_{1j}) q_j dA - \int \int_A (W_{,1})_{\text{expl}} q dA, \quad (i, j = 1, 2), \tag{7}$$

$$J_2 = \int \int_A (\sigma_{ij} u_{i,2} - W \delta_{2j}) q_j dA - \int \int_A (W_{,2})_{\text{expl}} q dA - \int_{\Gamma_c} (W^+ - W^-) q ds, \quad (i, j = 1, 2). \tag{8}$$

In the above representations, there are area integrals and a line integral, which are defined over  $A$  and  $\Gamma_c$ , respectively.  $A$  is an arbitrary area around the crack tip and  $\Gamma_c$  is a straight line corresponding to the portion of the crack lying in  $A$ . Both  $A$  and  $\Gamma_c$  are depicted in Fig. 2. In the present study, for simplicity, we make use of a circular area  $A$  of radius  $R$  as shown in this figure. The straight line  $\Gamma_c$  on the other hand is the line extending from point  $B$  to point  $O$ . Since, the  $J_k$ -integral is domain independent, the components  $J_1$  and  $J_2$  are independent of the radius  $R$  of the area  $A$ .

In Eqs. (7) and (8),  $\delta_{1j}$  and  $\delta_{2j}$  are Kronecker delta functions,  $W^+$  and  $W^-$  are the mechanical strain energy density functions defined over the upper and lower crack surfaces, respectively, and  $(W_{,1})_{\text{expl}}$  and  $(W_{,2})_{\text{expl}}$  are the explicit derivatives of the mechanical strain energy density function.  $q$  is a function of  $x_1$  and  $x_2$ , and represents a right circular cone of height unity. The base circle of the cone is centered at the origin  $O$ , and has a radius of  $R$ . The explicit derivatives of the mechanical strain energy density function depend on the partial derivatives of  $W$  with respect to the material parameters and the temperature difference, as well as the partial derivatives of the material parameters and the temperature difference with respect to the spatial coordinates. The expressions of  $(W_{,1})_{\text{expl}}$  for plane stress and strain are given in the paper by Dag (2006). For each case,  $(W_{,2})_{\text{expl}}$  can be easily derived by replacing  $x_1$  by  $x_2$  in the corresponding  $(W_{,1})_{\text{expl}}$  expression.

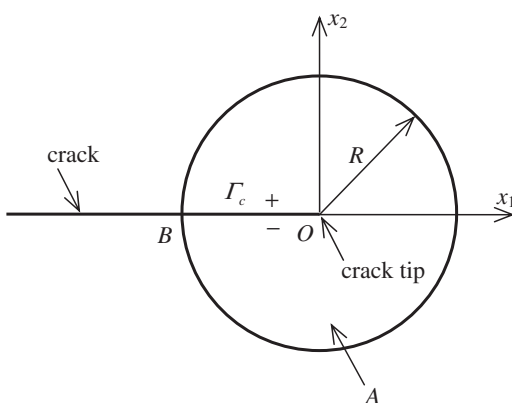


Fig. 2. Integration domains  $A$  and  $\Gamma_c$ .

The area integrals in  $J_1$  and  $J_2$  can be evaluated numerically in a straightforward manner by utilizing Gauss quadrature techniques. However, the line integral in  $J_2$  requires special treatment due to the square-root singular behavior of the mechanical strain energy density difference  $(W^+ - W^-)$  near the crack tip. Eischen (1987a) suggested that the integration interval of the line integral be divided into two parts, the first remote from the crack tip and the second close to the crack tip. The integral with the interval close to the crack tip can then be evaluated in closed form using the asymptotic approximation to the mechanical strain energy density difference. This approach is adopted in various studies and shown to lead to numerical results of high accuracy (Kim and Paulino, 2003; Dag and Yildirim, 2009). Following Eischen's method,  $J_2$  is written as

$$J_2 = \int \int_A (\sigma_{ij} u_{i,2} - W \delta_{2j}) q_j dA - \int \int_A (W_{,2})_{\text{expl}} q dA - \int_0^{R-d} (W^+ - W^-) q dx + 4 \sqrt{\frac{d}{2\pi}} \frac{b(3R-d)}{3R} K_{II} T_s, \quad (i, j = 1, 2). \tag{9}$$

In this equation,  $R$  is the length of the integration path  $\Gamma_c$ ,  $d$  is the length of the interval over which  $(W^+ - W^-)$  is approximated by its asymptotic representation,  $x$  is the variable of the line integral,  $b$  is a constant that depends on the material parameters evaluated at the crack tip, and  $T_s$  is the  $T$ -stress, i.e. the constant term in the asymptotic expansion of the stress component  $\sigma_{11}$ . The asymptotic form can accurately approximate  $(W^+ - W^-)$  only if  $d$  is sufficiently small compared to the crack length. A schematic of the integration path of the line integral is shown in Fig. 3.

### 3. Evaluation of the thermal fracture parameters

If for a mixed-mode crack problem, temperature, displacement, stress, and strain fields are known,  $J_1$  can be numerically evaluated by using Eq. (7). The expression of  $J_2$ , as given by Eq. (9) however, contains  $K_{II}$  and  $T_s$ , which are unknowns. In order to circumvent this difficulty, we first define a new quantity  $\hat{J}_2$  in the form:

$$\hat{J}_2 = \int \int_A (\sigma_{ij} u_{i,2} - W \delta_{2j}) q_j dA - \int \int_A (W_{,2})_{\text{expl}} q dA - \int_0^{R-d} (W^+ - W^-) q dx, \quad (i, j = 1, 2). \tag{10}$$

In the finite element implementation, for a given crack problem first  $\hat{J}_2$  is computed for two different values of  $d$ . If we denote these two different values of  $d$  and the corresponding values of  $\hat{J}_2$  respectively by  $d_1, d_2$  and  $\hat{J}_2^1, \hat{J}_2^2$ , we get

$$\hat{J}_2^1 = J_2 - \sqrt{d_1} \left(1 - \frac{d_1}{3R}\right) S, \quad \hat{J}_2^2 = J_2 - \sqrt{d_2} \left(1 - \frac{d_2}{3R}\right) S, \tag{11}$$

where,

$$S = \frac{4b}{\sqrt{2\pi}} K_{II} T_s. \tag{12}$$

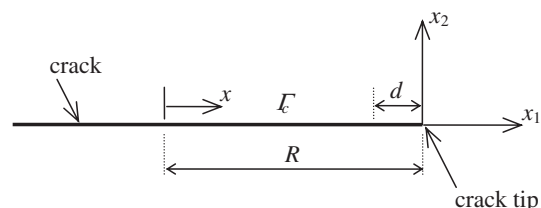


Fig. 3. Schematic of the integration path of the line integral.

Then,  $J_2$  and  $S$  are obtained by solving the linear system given by Eq. (11).

In order to compute the modes I and II stress intensity factors and the  $T$ -stress, we need the relations among these parameters, and the components of the  $J_k$ -integral. When one of the principal axes of orthotropy is parallel and the other is perpendicular to the crack plane as shown in Fig. 1, the relations between the SIFs and the components of the  $J_k$ -integral are as follows (Kim and Paulino, 2003):

$$J_1 = B_1 K_I^2 + B_2 K_{II}^2, \quad J_2 = B_3 K_I K_{II}, \quad (13)$$

where  $B_1$ ,  $B_2$ , and  $B_3$  are constants that depend on the material parameters evaluated at the crack tip. Eliminating  $K_{II}$  from the equations given above, we obtain  $K_I$  as,

$$K_I = \pm \sqrt{\frac{J_1}{2B_1} \left\{ 1 \pm \sqrt{1 - \frac{4B_1 B_2}{B_3^2} \left(\frac{J_2}{J_1}\right)^2} \right\}}. \quad (14)$$

Once  $K_I$  is calculated through Eq. (14),  $K_{II}$  can be found by using the  $J_2$  expression given in Eq. (13). The  $T$ -stress can then be computed via Eq. (12). The correct value of  $K_I$  among the four possible values given by Eq. (14) is determined by adopting the decoupling technique outlined by Sollero and Aliabadi (1993). This decoupling technique is based on the use of the relative normal and tangential displacements of two nodes located close to the crack tip.

#### 4. Finite element implementation

The developed  $J_k$ -integral based technique is implemented by means of the finite element method. The procedure described in Section 3 is integrated into the general purpose finite element analysis software ANSYS (1997). The first step in thermal fracture analysis of orthotropic FGMs is the computation of the temperature field. For the graded orthotropic medium depicted in Fig. 1, the two-dimensional transient temperature distribution can be found by solving the heat equation which is in the form:

$$\frac{\partial}{\partial x_1} \left( k_1(x_1, x_2) \frac{\partial T}{\partial x_1} \right) + \frac{\partial}{\partial x_2} \left( k_2(x_1, x_2) \frac{\partial T}{\partial x_2} \right) = \rho c_h \frac{\partial T}{\partial t}. \quad (15)$$

In Eq. (15),  $T$  is the temperature,  $k_1$ ,  $k_2$  are the principal thermal conductivities in  $x_1$  and  $x_2$  directions, respectively,  $\rho$  is the density,  $c_h$  is the specific heat, and  $t$  is the time. For a given crack configuration, this equation is solved by using ANSYS and the resulting temperature field is provided as an input to the mechanical analysis. The displacements, strains, and stresses computed through the mechanical analysis are used in the evaluation of the thermal fracture parameters. In both thermal and mechanical analyses, identical finite element meshes are utilized. The finite element meshes used comprise 6-noded triangular elements. A 6-noded triangle is formed by merging the three nodes of an 8-noded quadrilateral element at a single point (Dag and Yildirim, 2009). The area and line integrals given in Eqs. (7) and (10) are computed by making use of the isoparametric finite element concept and standard Gauss quadrature techniques.

In the technical literature, two basic approaches are utilized to compute the material properties of FGMs. In the first approach, the physical properties are represented by certain continuous functions of spatial coordinates. In the second approach, micromechanics models are used to estimate the material parameters. Among the commonly used micromechanics models for FGMs, we can mention the standard micromechanics approaches such as the self-consistent method (Hill, 1965), and the Mori–Tanaka method (Mori and Tanaka, 1973); and the higher-order micromechanical theories, which explicitly couple the microstructural and the

macrostructural effects (Aboudi et al., 1999). The aim in the present study is to develop a finite element method, which – given the material property variations – can be used to predict thermal fracture parameters for orthotropic FGMs. The method is developed in a way that, it yields the accurate crack tip parameters regardless of the particular types of material property variation profiles. The employment of micromechanics models to estimate these material property variation profiles is not within the scope of our study. As described in the next section, we used power functions to represent the spatial variations of the material properties of orthotropic FGMs. The use of power functions for modeling of the material property variation profiles of FGMs is a widely accepted and used approach in the technical literature (Li, 2008; Woo et al., 2006; Shen, 2002; Lee and Erdogan, 1998).

There are two different ways of taking into account the smooth spatial variations of the material properties of FGMs in a finite element model. The elements used in these two different methods are named as graded and homogeneous finite elements. During the formation of the element stiffness matrix of a graded finite element, the material parameters are computed at each Gauss point (Dag, 2006). For a homogeneous finite element however, the material parameters are uniform and computed at the centroid (Dag and Ilhan, 2008). Both approaches lead to numerical results of high accuracy provided that the finite element mesh possesses adequate refinement in the crack tip region. In the current study, we employ homogeneous finite elements to model the smooth spatial variations of the thermomechanical properties of orthotropic FGMs.

As indicated by Eq. (11), the  $d$  values used to determine  $\widehat{J}_1^2$  and  $\widehat{J}_2^2$  are denoted by  $d_1$  and  $d_2$ . It is required that  $d_1$  and  $d_2$  be sufficiently small, since they are the lengths of the regions in which  $(W^+ - W^-)$  is approximated by its asymptotic representation. Our numerical studies showed that the developed computational procedure yields accurate results when  $d_1$  and  $d_2$  are set such that,  $d_1 = 2(10)^{-5}a$  and  $d_2 = 6(10)^{-5}a$ , where  $a$  is the half crack length.

#### 5. Numerical results

In this section, we consider two different crack problems in order to illustrate the application of the developed  $J_k$ -integral based method. The first problem we examine is that of an embedded crack located in an orthotropic FGM layer subjected to steady-state thermal stresses. In the second case, we deal with a periodic cracking problem for which mixed-mode transient fracture parameters were previously evaluated by Dag et al. (2007) through the use of enriched finite elements.

The geometry of the first problem is shown in Fig. 4.  $X_1$  and  $X_2$  in the figure are the principal and at the same time the global coordinates. The orthotropic FGM layer has a thickness of  $h$  and contains an embedded crack of length  $2a$  located at  $X_2 = h_1$ . The layer is assumed to be 100% metal at  $X_2 = 0$  and 100% ceramic at  $X_2 = h$ . The metal and ceramic components of the FGM layer are nickel (Ni) and alumina ( $Al_2O_3$ ), respectively. The layer is orthotropic and there are smooth spatial variations in all of the thermomechanical properties in the thickness direction. Hence, all thermomechanical properties are functions of the  $X_2$ -coordinate.

The elastic medium is assumed to be initially at a reference temperature of  $T_0$  for which the stresses are zero. The temperature of the bounding plane at  $y = h$  is then increased to  $2T_0$  and that of the boundary at  $y = 0$  is kept at  $T_0$ . The crack surfaces and all other bounding planes are taken as insulated. It is further assumed that steady-state temperature field is established within the layer. Under these conditions, the heat flow is two-dimensional and the temperature field can be computed by taking the right hand side of Eq. (15) as zero. The continuous variations in the thermomechanical

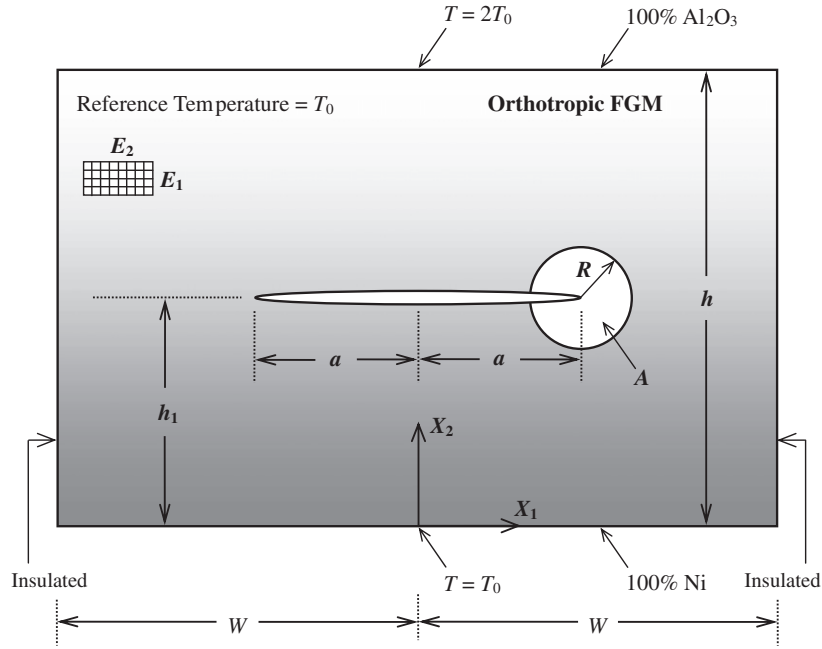


Fig. 4. An embedded crack in an orthotropic FGM layer.

properties of the layer are represented by power functions; and each of the material properties required in the steady-state analysis is expressed in the following form:

$$A(X_2) = A^m + (A^c - A^m) \left( \frac{X_2}{h} \right)^p, \quad (16)$$

where  $A$  stands for any of the material parameters, and the superscripts  $m$  and  $c$  refer to the properties of the 100% metal (Ni) and 100% ceramic ( $\text{Al}_2\text{O}_3$ ) planes, respectively. The variation given above is used for the material parameters  $E_1$ ,  $E_2$ ,  $\nu_{12}$ ,  $\nu_{13}$ ,  $\nu_{31}$ ,  $\nu_{32}$ ,  $G_{12}$ ,  $\alpha_1$ ,  $\alpha_2$ ,  $\alpha_3$ ,  $k_1$ , and  $k_2$ . The corresponding exponents for these properties are respectively denoted by  $\gamma_1$ ,  $\gamma_2$ ,  $\beta_{12}$ ,  $\beta_{13}$ ,  $\beta_{31}$ ,  $\beta_{32}$ ,  $\gamma_{12}$ ,  $\delta_1$ ,  $\delta_2$ ,  $\delta_3$ ,  $\omega_1$ , and  $\omega_2$ .

Alumina–nickel is a commonly used combination in the processing of ceramic–metal functionally graded materials (Bhattacharyya et al., 2008; Krufft et al., 2008). An alumina–nickel FGM coating can be processed by employing the plasma spray forming technique, and depositing alumina and nickel over a metallic substrate (Kesler et al., 1998). The deposited coating would be 100% alumina at the free surface and 100% nickel at the interface. Due to the use of plasma spray forming, such a coating is expected to be both orthotropic and nonhomogeneous. Experimental data on the orthotropic elastic and conductive properties of plasma-sprayed orthotropic alumina is available in the articles by Parthasarathi et al. (1995), and Sevostianov and Kachanov (2001); and we used this data for the elastic and conductive properties of the 100% alumina surface. However, no published data is available in the literature on the orthotropic thermal expansion coefficients of plasma-sprayed alumina. The nominal value for the thermal expansion coefficient of alumina is given as  $\alpha = 7.5(10)^{-6} (\text{°C})^{-1}$  by Callister (2000). This value is used as the thickness-direction thermal expansion coefficient of the 100% alumina surface. For the other two principal directions, larger values are used in order to be able to assess the influence of orthotropy on the fracture mechanics parameters. The density and specific heat of alumina are also taken from the reference, Callister (2000). The thermoelastic properties of the 100% alumina surface are then given as

$$E_1^c = 90.43 \text{ GPa}, E_2^c = 116.36 \text{ GPa}, G_{12}^c = 38.21 \text{ GPa}, \quad (17)$$

$$\nu_{12}^c = 0.22, \nu_{13}^c = 0.14, \nu_{31}^c = 0.14, \nu_{32}^c = 0.21, \quad (18)$$

$$\alpha_1^c = 8(10)^{-6} (\text{°C})^{-1}, \alpha_2^c = 7.5(10)^{-6} (\text{°C})^{-1}, \alpha_3^c = 9(10)^{-6} (\text{°C})^{-1}, \quad (19)$$

$$k_1^c = 21.25 \text{ W}/(\text{m K}), k_2^c = 29.82 \text{ W}/(\text{m K}), \quad (20)$$

$$\rho^c = 3980 \text{ kg}/\text{m}^3, C_h^c = 775 \text{ J}/(\text{kg K}). \quad (21)$$

The data used for the property values of the 100% nickel surface is from Callister (2000) and provided below

$$E_1^m = E_2^m = E^m = 204 \text{ GPa}, \nu_{12}^m = \nu_{13}^m = \nu_{31}^m = \nu_{32}^m = \nu^m = 0.31, \quad (22)$$

$$G_{12}^m = E^m / (2(1 + \nu^m)) = 77.9 \text{ GPa}, \alpha_1^m = \alpha_2^m = \alpha_3^m = 13.3(10)^{-6} (\text{°C})^{-1}, \quad (23)$$

$$k_1^m = k_2^m = 70 \text{ W}/(\text{m K}), \quad (24)$$

$$\rho^m = 8890 \text{ kg}/\text{m}^3, C_h^m = 456 \text{ J}/(\text{kg K}). \quad (25)$$

Eqs. (16)–(25) are approximate since the metallic microstructure in the FGM layer could also be orthotropic. Although, the density and specific heat values given by Eqs. (21) and (25) are not required in the solution of the steady-state problem described above, they are needed in the transient thermal fracture analysis elucidated at the end of this section. Note also that there are limitations on the Poisson's ratios of orthotropic materials as indicated by Agarwal and Broutman (1990); and these limitations are satisfied at every point of the orthotropic functionally graded layer.

The loading and the geometry are both symmetric about  $X_2$ -axis for the problem shown in Fig. 4. The vertical displacement and the temperature are even functions of  $X_1$  while the horizontal displacement is an odd function of the same coordinate. It suffices to construct a finite element model of one-half of the medium. Hence, the finite element model is developed for the domain  $X_1 \geq 0$  and the fracture parameters are computed at the crack tip  $X_1 = a$ . The parameters at the tip  $X_1 = -a$  can be obtained by considering the equalities

$$J_1(a) = J_1(-a), \quad J_2(a) = -J_2(-a), \quad (26)$$

$$K_{I}(a) = K_{I}(-a), \quad K_{II}(a) = -K_{II}(-a), \quad T_s(a) = T_s(-a). \quad (27)$$

A circular domain of radius  $R$  is used to conduct fracture analysis at the tip  $X_1 = a$ . The domain geometry is also depicted in Fig. 4. The finite element meshes used in the solutions of the thermal and mechanical problems are identical and comprise 6-noded triangular elements.

In order to validate the developed  $J_k$ -integral based method, some comparisons of the numerical results obtained by  $J_k$ -integral are made to those computed by using another computational method, namely the displacement correlation technique. The normalized modes I and II stress intensity factors evaluated at the crack tip  $X_1 = a$  by these two different methods are provided in Table 1. The normalized SIFs are defined as

$$K_{In} = \frac{K_I}{\sigma_0 \sqrt{\pi a}}, \quad K_{II n} = \frac{K_{II}}{\sigma_0 \sqrt{\pi a}}, \quad \sigma_0 = \alpha_1^c E_1^c T_0. \quad (28)$$

The details of the displacement correlation technique for mixed-mode fracture analysis of orthotropic FGMs are provided by Dag and Ilhan (2008) and not given here for brevity. The stress intensity factors shown in the table are generated by considering both plane stress and strain and by taking  $\delta_2$  as 1/3 and 3.  $\delta_2$  is the exponent of the power function representing the variation of the thermal expansion coefficient  $\alpha_2$ . Four different values of the normalized radius  $R/a$  are used to compute the SIFs by the  $J_k$ -integral method. The deformed shape of the finite element mesh used in the analyses carried out for the case of plane strain and  $\delta_2 = 3$  is given in Fig. 5. This mesh contains a total of 93952 triangular elements and 189,223 nodes. From Table 1, it can be seen that the results calculated for the four different values of  $R/a$  are in excellent agreement. This demonstrates the domain independence of the developed form of the  $J_k$ -integral. The results generated by the  $J_k$ -integral also agree quite well with those evaluated by using DCT, which is indicative of the high levels of accuracy achieved by both methods.

Figs. 6–8 show the variations of the steady-state normalized fracture parameters calculated at the crack tip  $X_1 = a$ , with respect to  $\omega_2$  and  $h_1/W$ .  $\omega_2$  is the exponent of the power function representing the variation of the thermal conductivity  $k_2$ . The SIFs given in Fig. 6 are normalized as shown by Eq. (28), while the energy release rate and the  $T$ -stress given respectively in Figs. 7 and 8 are normalized as

$$J_{1n} = \frac{J_1}{\frac{\sigma_0^2 \pi a}{E_1^c} (1 - (\nu_{12}^c)^2)}, \quad T_{sn} = \frac{T_s}{\sigma_0}, \quad (29)$$

where  $\sigma_0$  follows from Eq. (28). The results are generated by considering the state of plane strain and taking  $R/a$  as 0.1. Double scales are utilized in the figures in order to more clearly present the influence of  $\omega_2$  on the crack tip parameters.  $\omega_2$  is varied between 0 and 1, and  $1/\omega_2$  is varied between 1 and 0 so as to cover the whole range  $0 \leq \omega_2 < \infty$  in a compact manner. The smallest value of  $h_1/W$  is taken as 0.2 since it is found that the surfaces of the crack come into contact and crack closure occurs for smaller values of  $h_1/W$ .

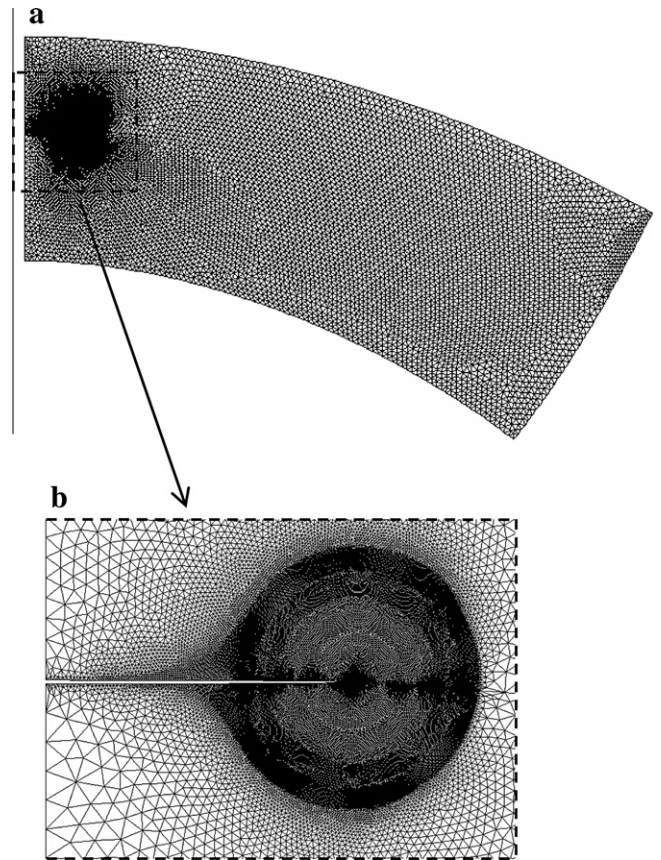


Fig. 5. (a) Deformed shape of the finite element mesh generated by considering the case of plane strain; (b) close-up view of the circular domains around the crack tip.  $a/W = 0.1$ ,  $h/W = 0.4$ ,  $h_1/W = 0.25$ ,  $\gamma_1 = \gamma_2 = \gamma_{12} = 2$ ,  $\beta_{12} = \beta_{13} = \beta_{31} = \beta_{32} = 1.5$ ,  $\delta_1 = \delta_2 = \delta_3 = 3$ ,  $\omega_1 = \omega_2 = 4$ .

Fig. 6 depicts the plots of the normalized modes I and II stress intensity factors,  $K_{In}$  and  $K_{II n}$ , as functions of  $\omega_2$  and  $h_1/W$ . Among the four considered values of  $h_1/W$ , 0.2 leads to the smallest  $K_{In}$ s. The  $K_{In}$  values evaluated for  $h_1/W = 0.3$  are slightly larger than those computed for  $h_1/W = 0.35$  when  $1/\omega_2$  is close to zero. Other than this exception,  $K_{In}$  is seen to increase as  $h_1/W$  is increased from 0.2 to 0.35 while  $\omega_2$  is kept constant.  $K_{II n}$  on the other hand, decreases as  $h_1/W$  increases from 0.2 to 0.35. In general, mode II SIFs are larger than the mode I SIFs implying the dominance of shear-mode deformation near the crack tips. Fig. 7 shows the effects of  $\omega_2$  and  $h_1/W$  on the normalized  $J_1$ -integral  $J_{1n}$ , which is equal to the normalized energy release rate. As  $h_1/W$  increases from 0.2 to 0.35, the normalized energy release rate decreases. It is also seen that  $J_{1n}$  is an increasing function of the exponent  $\omega_2$ . The results illustrating the effects of  $\omega_2$  and  $h_1/W$  on the

Table 1

Comparisons of the stress intensity factors obtained by  $J_k$ -integral to those calculated by DCT.  $a/W = 0.1$ ,  $h/W = 0.4$ ,  $h_1/W = 0.25$ ,  $\gamma_1 = \gamma_2 = \gamma_{12} = 2$ ,  $\beta_{12} = \beta_{13} = \beta_{31} = \beta_{32} = 1.5$ ,  $\delta_1 = \delta_3 = 3$ ,  $\omega_1 = \omega_2 = 4$ .

|              |                  |            | $J_k$ -integral |             |             |             | DCT    |
|--------------|------------------|------------|-----------------|-------------|-------------|-------------|--------|
|              |                  |            | $R/a = 0.1$     | $R/a = 0.2$ | $R/a = 0.3$ | $R/a = 0.4$ |        |
| Plane stress | $\delta_2 = 1/3$ | $K_{In}$   | 0.0176          | 0.0176      | 0.0176      | 0.0176      | 0.0177 |
|              |                  | $K_{II n}$ | 0.1197          | 0.1197      | 0.1197      | 0.1197      | 0.1190 |
|              | $\delta_2 = 3$   | $K_{In}$   | 0.0207          | 0.0207      | 0.0207      | 0.0207      | 0.0209 |
|              |                  | $K_{II n}$ | 0.1271          | 0.1271      | 0.1271      | 0.1271      | 0.1263 |
| Plane strain | $\delta_2 = 1/3$ | $K_{In}$   | 0.0259          | 0.026       | 0.026       | 0.0261      | 0.0259 |
|              |                  | $K_{II n}$ | 0.1586          | 0.1587      | 0.1588      | 0.1589      | 0.1579 |
|              | $\delta_2 = 3$   | $K_{In}$   | 0.0294          | 0.0295      | 0.0295      | 0.0296      | 0.0294 |
|              |                  | $K_{II n}$ | 0.1663          | 0.1664      | 0.1665      | 0.1666      | 0.1656 |

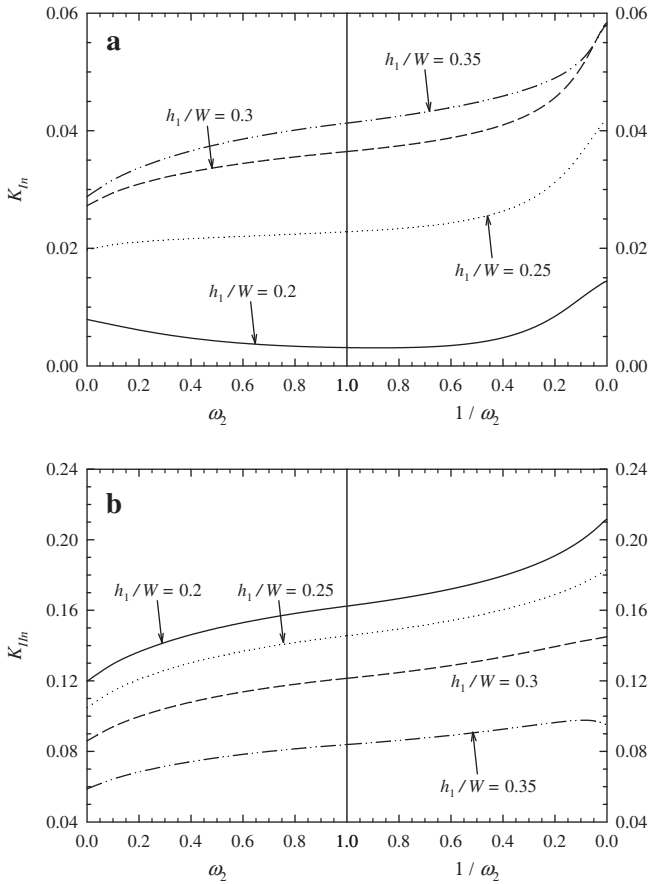


Fig. 6. Normalized mixed-mode stress intensity factors versus  $\omega_2$  and  $h_1/W$ : (a) mode I SIFs; (b) mode II SIFs.  $a/W=0.1$ ,  $h/W=0.4$ ,  $\gamma_1 = \gamma_2 = \gamma_{12} = 2$ ,  $\beta_{12} = \beta_{13} = \beta_{31} = \beta_{32} = 1.5$ ,  $\delta_1 = \delta_2 = \delta_3 = 3$ ,  $\omega_1 = 4$ .

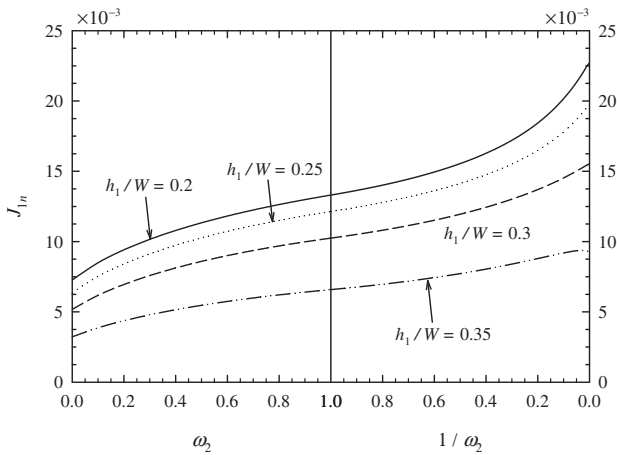


Fig. 7. Normalized energy release rate versus  $\omega_2$  and  $h_1/W$ .  $a/W=0.1$ ,  $h/W=0.4$ ,  $\gamma_1 = \gamma_2 = \gamma_{12} = 2$ ,  $\beta_{12} = \beta_{13} = \beta_{31} = \beta_{32} = 1.5$ ,  $\delta_1 = \delta_2 = \delta_3 = 3$ ,  $\omega_1 = 4$ .

normalized  $T$ -stress  $T_{sn}$  are provided in Fig. 8. The  $T$ -stress can be tensile or compressive depending on the values of  $\omega_2$  and  $h_1/W$ .  $T_s$  is found to be tensile for  $h_1/W=0.35$  and compressive for  $h_1/W=0.2, 0.25$  and  $0.3$ . Furthermore, the  $T_{sn}$  curve goes through a maximum when  $h_1/W=0.2$  or  $0.25$  and a minimum when  $h_1/W=0.35$ .

The second problem we consider to validate the  $J_k$ -integral based method is the problem of periodic cracking in an orthotropic

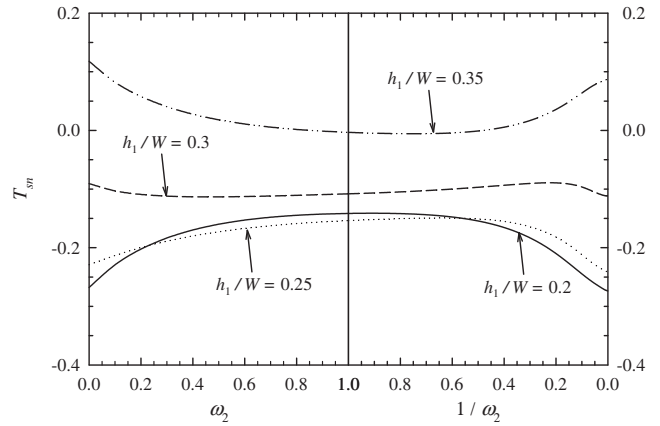


Fig. 8. Normalized  $T$ -stress versus  $\omega_2$  and  $h_1/W$ .  $a/W=0.1$ ,  $h/W=0.4$ ,  $\gamma_1 = \gamma_2 = \gamma_{12} = 2$ ,  $\beta_{12} = \beta_{13} = \beta_{31} = \beta_{32} = 1.5$ ,  $\delta_1 = \delta_2 = \delta_3 = 3$ ,  $\omega_1 = 4$ .

FGM layer that is subjected to transient thermal stresses. Mixed-mode stress intensity factors for this case were originally provided in the article by Dag et al. (2007). These results were computed by utilizing enriched finite elements at the crack tip. The geometry of the problem is depicted in Fig. 9. An infinitely long FGM layer of thickness  $h$  possesses periodic cracks of length  $2a$  and spacing  $W$ ; and is assumed to be in a deformation state of plane strain. The layer is initially stress-free at a reference temperature of  $T_0$ . The temperature of the boundary at  $X_2 = h - h_1$  is then increased to  $2T_0$  and that of the boundary at  $X_2 = -h_1$  is kept at  $T_0$ . The surfaces of all cracks are insulated. The transient temperature field under these boundary conditions is determined by solving Eq. (15).

All thermomechanical properties of the layer are continuously variable in  $X_2$ -direction. The bounding planes at  $X_2 = h - h_1$  and  $X_2 = -h_1$  are assumed to be 100% alumina and 100% nickel, respectively. The variations in the material parameters are represented by power functions. Each of the material properties has the following functional form (Dag et al., 2007):

$$B(X_2) = B^c + (B^m - B^c) \left( \frac{h - h_1 - X_2}{h} \right)^q, \quad (30)$$

where  $B$  symbolizes any of the material properties. The superscript  $c$  refers to the 100% ceramic (alumina) plane at  $X_2 = h - h_1$  whereas  $m$  refers to the 100% metal (nickel) plane at  $X_2 = -h_1$ . The properties of the 100% ceramic and 100% metal planes are given by Eqs. (17)–(25). In the analysis presented by Dag et al. (2007), the variation given by the above equation is applied to the material parameters  $E_1, E_2, \nu_{21}, \nu_{23}, \nu_{31}, \nu_{32}, G_{12}, \alpha_1, \alpha_2, \alpha_3, k_1, k_2, \rho$ , and  $C_h$ ; and the exponents corresponding to these parameters are respectively denoted by  $\gamma_1, \gamma_2, \beta_{21}, \beta_{23}, \beta_{31}, \beta_{32}, \gamma_{12}, \delta_1, \delta_2, \delta_3, \omega_1, \omega_2, \lambda$ , and  $\chi$ . The finite

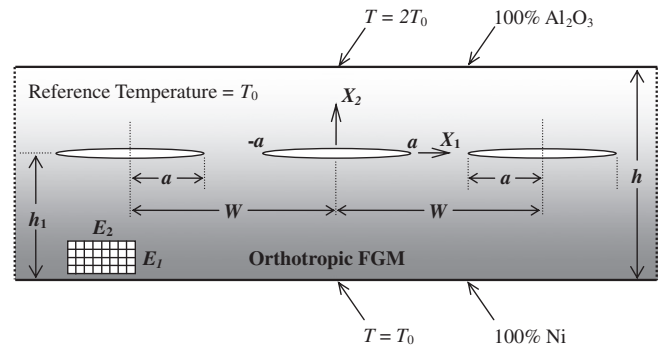


Fig. 9. Periodic cracks in an orthotropic FGM layer.

**Table 2**

Comparisons of the transient stress intensity factors computed by  $J_k$ -integral to those given by Dag et al. (2007).  $a/W = 0.3$ ,  $h/W = 0.6$ ,  $h_1/W = 0.5$ ,  $\gamma_1 = \gamma_2 = \gamma_{12} = 2$ ,  $\beta_{21} = \beta_{23} = \beta_{31} = \beta_{32} = 1.5$ ,  $\delta_1 = \delta_2 = \delta_3 = 2$ ,  $\omega_1 = \omega_2 = 2$ ,  $\lambda = \chi = 1.5$ .

| $\tau$ | $J_k$ -integral |           | Dag et al. (2007) |           |
|--------|-----------------|-----------|-------------------|-----------|
|        | $K_{In}$        | $K_{IIn}$ | $K_{In}$          | $K_{IIn}$ |
| 0.01   | 0.0524          | 0.0757    | 0.0526            | 0.0761    |
| 0.015  | 0.0619          | 0.0978    | 0.0625            | 0.0987    |
| 0.02   | 0.0689          | 0.1105    | 0.0694            | 0.1114    |
| 0.03   | 0.0771          | 0.1221    | 0.0778            | 0.1225    |
| 0.04   | 0.0813          | 0.1248    | 0.0820            | 0.1257    |

element solution of the periodic cracking problem requires that, finite element model of a unit cell be generated by imposing appropriate boundary and periodicity conditions. Extensive details on finite element modeling of periodic cracks are available in the paper by Dag et al. (2007).

The comparisons of the transient normalized modes I and II stress intensity factors computed by means of  $J_k$ -integral to those given by Dag et al. (2007) are provided in Table 2.  $R/a$  value is fixed as 0.05 in the  $J_k$ -integral computations. Since  $h_1/W$  is set as 0.5, the crack tip is in the proximity of the upper boundary  $X_2 = h - h_1$ . For this reason, it was possible to use only a relatively small value for  $R/a$ . In Table 2,  $\tau$  stands for normalized time and defined as

$$\tau = \frac{k_1^c}{\rho^c C_h^c h^2} t. \quad (31)$$

The definitions of the normalized mixed-mode SIFs,  $K_{In}$  and  $K_{IIn}$ , are same as those shown by Eq. (28).

Examining the results given in the table, it can be seen that the normalized modes I and II stress intensity factors generated by the  $J_k$ -integral based method are in very good agreement with those given by Dag et al. (2007). Therefore, considering the validation studies described in this section, we conclude that the developed form of the  $J_k$ -integral is domain independent; and that the proposed computational technique is a robust way of evaluating fracture parameters for orthotropic FGMs that are subjected to steady-state or transient thermal stresses.

## 6. Concluding remarks

In this article, a new computational method based on the  $J_k$ -integral is introduced, which enables accurate evaluation of fracture parameters for orthotropic FGMs subjected to thermal stresses. A finite element procedure is put forward so as to compute the modes I and II stress intensity factors, the energy release rate, and the  $T$ -stress. The developed method is validated on two different fracture mechanics problems: The problem of an embedded crack in an orthotropic FGM layer under steady-state thermal stresses; and that of periodic cracks subjected to transient thermal loading. Comparisons provided by considering these two problems do point out that, the proposed form of the  $J_k$ -integral possesses the required domain independence and leads to numerical results of high accuracy.

A numerical analysis is conducted by considering the embedded crack problem in order to assess the effects of the relative crack location  $h_1/W$  and the exponent  $\omega_2$ . It is shown that the relative crack location strongly influences the outcome of the fracture analysis. Crack closure is found to occur for  $h_1/W$  values less than 0.2; hence in the computations minimum  $h_1/W$  value is set as 0.2 to avoid the contact of the crack surfaces. The numerical results presented also demonstrate the variations of the crack tip parameters with respect to the exponent  $\omega_2$ , which governs the gradation profile of the thermal conductivity in the thickness direction. It is

shown that the normalized energy release rate is an increasing function of  $\omega_2$ . This exponent is also found to have a significant influence on the  $T$ -stress.

The method presented in this article has certain advantages over other computational techniques used in fracture analysis of FGMs, which can be exploited to conduct a more effective analysis. For example, in the displacement correlation technique (Dag and Ilhan, 2008) and the enriched finite element method (Dag et al., 2007), special crack tip elements are needed to extract the mixed-mode stress intensity factors; however, the proposed method does not require the use of special crack tip elements for the evaluation of the fracture parameters. One other computational technique developed previously for fracture analysis of orthotropic functionally graded materials is based on the interaction integral (Kim and Kc, 2008). In the interaction integral approach, the  $J$ -integral is used in conjunction with auxiliary fields, which have to be suitably defined in order to evaluate the crack tip parameters. On the other hand, in the formulation of the  $J_k$ -integral, auxiliary fields are not required and the generalized definition can be directly reduced to a form defined over finite domains. The interaction integral is expressed in terms of solely area integrals (Kim and Kc, 2008) whereas the domain independent form of the  $J_k$ -integral comprises both area and line integrals. Nevertheless, the existence of the line integral term in the  $J_k$ -integral expression is not deemed to be a particular disadvantage, since this integral can be evaluated quite accurately by utilizing the method described in Section 2.

In the finite element implementation of the  $J_k$ -integral method, a high degree of mesh refinement is required especially in the vicinity of the crack tip and in the domain over which  $J_k$ -integral is defined. This results in the utilization of a large number of elements in the finite element model. However, all the elements used in the discretization of the medium are regular finite elements. For this reason, the construction of the finite element mesh becomes relatively straightforward with a general purpose finite element analysis software such as ANSYS.

The work reported in this article is original in the sense that it illustrates how the  $J_k$ -integral can be formulated and implemented using the finite element method to compute thermal fracture parameters for orthotropic functionally graded materials. The  $J_k$ -integral based procedure proposed allows direct calculation of not only the mixed-mode stress intensity factors and the energy release rate but also the  $T$ -stress. The inclusion of the  $T$ -stress in computations aimed at determining crack kinking angles or crack tip plastic zone sizes is known to enhance the accuracy of the generated results. The analysis capability developed in the present study is seen to be particularly suited for quantifying the influences of material property variation profiles upon the fracture parameters. This capability can also be incorporated into optimization schemes in order to determine the composition profiles of orthotropic functionally graded components that will minimize the thermally induced crack driving forces.

## References

- Aboudi, J., Pindera, M.-J., Arnold, S.M., 1999. Higher-order theory for functionally graded materials. *Compos. B Eng.* 30, 777–832.
- Agarwal, B.D., Broutman, L.J., 1990. *Analysis and Performance of Fiber Composites*, second ed. John Wiley and Sons, New York, NY, USA.
- ANSYS, 1997. *ANSYS Basic Analysis Procedures Guide*, release 5.4. ANSYS Inc., Canonsburg, PA, USA.
- Bhattacharyya, M., Kumar, A.N., Kapuria, S., 2008. Synthesis and characterization of Al/SiC and Ni/Al<sub>2</sub>O<sub>3</sub> functionally graded materials. *Mater. Sci. Eng. A – Struct.* 487, 524–535.
- Budiansky, B., Rice, J.R., 1973. Conservation laws and energy-release rates. *J. Appl. Mech.* – *Trans. ASME* 40, 201–205.
- Callister, W.D., 2000. *Materials Science and Engineering: An Introduction*, fifth ed. John Wiley and Sons, New York, NY, USA.
- Chen, W.-H., Chen, K.-T., 1981. On the study of mixed-mode thermal fracture using modified  $J_k$  integrals. *Int. J. Fract.* 17, R99–R103.

- Chen, W.-H., Ting, K., 1985. Finite element analysis of mixed-mode thermoelastic fracture problems. *Nucl. Eng. Des.* 90, 55–65.
- Chu, S.J., Hong, C.S., 1990. Application of the  $J_k$  integral to mixed mode crack problems for anisotropic composite laminates. *Eng. Fract. Mech.* 35, 1093–1103.
- Dag, S., 2006. Thermal fracture analysis of orthotropic functionally graded materials using an equivalent domain integral approach. *Eng. Fract. Mech.* 73, 2802–2828.
- Dag, S., 2007. Mixed-mode fracture analysis of functionally graded materials under thermal stresses: a new approach using  $J_k$ -integral. *J. Therm. Stresses* 30, 269–296.
- Dag, S., Ilhan, K.A., 2008. Mixed-mode fracture analysis of orthotropic functionally graded material coatings using analytical and computational methods. *J. Appl. Mech.* – Trans. ASME 75, 051104.
- Dag, S., Yildirim, B., 2009. Computation of thermal fracture parameters for inclined cracks in functionally graded materials using  $J_k$ -integral. *J. Therm. Stresses* 32, 530–556.
- Dag, S., Yildirim, B., Sarikaya, D., 2007. Mixed-mode fracture analysis of orthotropic functionally graded materials under mechanical and thermal loads. *Int. J. Solids Struct.* 44, 7816–7840.
- Eischen, J.W., 1987a. An improved method for computing the  $J_2$  integral. *Eng. Fract. Mech.* 26, 691–700.
- Eischen, J.W., 1987b. Fracture of nonhomogeneous materials. *Int. J. Fract.* 34, 3–22.
- Hellen, T.K., Blackburn, W.S., 1975. The calculation of stress intensity factors for combined tensile and shear loading. *Int. J. Fract.* 11, 605–617.
- Hill, R., 1965. A self-consistent mechanics of composite materials. *J. Mech. Phys. Solids* 13, 213–222.
- Kawasaki, A., Watanabe, R., 2002. Thermal fracture behavior of metal/ceramic functionally graded materials. *Eng. Fract. Mech.* 69, 1713–1728.
- Kaysser, W.A., Ilchner, B., 1995. FGM research activities in Europe. *MRS Bull.* 20, 22–26.
- Kesler, O., Matejicek, J., Sampath, S., Suresh, S., Gnaeupel-Herold, T., Brand, P.C., Prask, H.J., 1998. Measurement of residual stress in plasma-sprayed metallic, ceramic and composite coatings. *Mater. Sci. Eng. A – Struct.* 487, 215–224.
- Kim, J.-H., Kc, A., 2008. A generalized interaction integral method for the evaluation of the  $T$ -stress in orthotropic functionally graded materials under thermal loading. *J. Appl. Mech.* – Trans. ASME 75, 051112.
- Kim, J.-H., Paulino, G.H., 2002. Finite element evaluation of mixed mode stress intensity factors in functionally graded materials. *Int. J. Numer. Methods Eng.* 53, 1903–1935.
- Kim, J.-H., Paulino, G.H., 2003. Mixed-mode  $J$ -integral formulation and implementation using graded finite elements for fracture analysis of nonhomogeneous orthotropic materials. *Mech. Mater.* 35, 107–128.
- Kim, J.-H., Paulino, G.H., 2004.  $T$ -stress in orthotropic functionally graded materials: Lekhnitskii and Stroh formalisms. *Int. J. Fract.* 126, 345–384.
- Knowles, J.K., Sternberg, E., 1972. On a class of conservation laws in linearized and finite elastostatics. *Arch. Ration. Mech. Anal.* 44, 187–211.
- Kruft, J.G., Bruck, H.A., Shabana, Y.M., 2008. Effect of TiO<sub>2</sub> nanopowder on the sintering behavior of nickel–alumina composites for functionally graded materials. *J. Am. Ceram. Soc.* 91, 2870–2877.
- Lee, Y.D., Erdogan, F., 1998. Interface cracking of FGM coatings under steady-state heat flow. *Eng. Fract. Mech.* 59, 361–380.
- Li, X.-F., 2008. A unified approach for analyzing static and dynamic behaviors of functionally graded Timoshenko and Euler–Bernoulli beams. *J. Sound Vib.* 318, 1210–1229.
- Liu, Y., Compson, C., Liu, M., 2004. Nanostructured and functionally graded cathodes for intermediate solid oxide fuel cells. *J. Power Sources* 138, 194–198.
- Mori, T., Tanaka, K., 1973. Average stress in matrix and average elastic energy of materials with misfitting inclusions. *Acta Mater.* 21, 571–574.
- Nomura, T., Moriguchi, H., Tsuda, K., Isobe, K., Ikegaya, A., Moriyama, K., 1999. Material design method for the functionally graded cemented carbide tool. *Int. J. Refract. Metals Hard Mater.* 17, 397–404.
- Ozturk, M., Erdogan, F., 1997. Mode I crack problem in an inhomogeneous orthotropic medium. *Int. J. Eng. Sci.* 35, 869–883.
- Pan, E., Amadei, B., 1996. Fracture mechanics of cracked 2-D anisotropic media with a new formulation of the boundary element method. *Int. J. Fract.* 77, 161–174.
- Parthasarathi, S., Tittmann, B.R., Sampath, K., Onesto, E.J., 1995. Ultrasonic characterization of elastic anisotropy in plasma sprayed alumina coatings. *J. Therm. Spray Technol.* 4, 367–373.
- Rice, J.R., 1968. A path independent integral and the approximate analysis of strain concentration by notches and cracks. *J. Appl. Mech.* – Trans. ASME 35, 379–386.
- Sampath, S., Herman, H., Shimoda, N., Saito, T., 1995. Thermal spray processing of FGMs. *MRS Bull.* 20, 27–31.
- Sevostianov, I., Kachanov, M., 2001. Plasma-sprayed ceramic coatings: anisotropic elastic and conductive properties in relation to microstructure; cross-property correlations. *Mater. Sci. Eng. A – Struct.* 297, 235–243.
- Shen, H.S., 2002. Postbuckling analysis of axially loaded functionally graded cylindrical panels in thermal environments. *Int. J. Solids Struct.* 39, 5991–6010.
- Sollero, P., Aliabadi, M.H., 1993. Fracture mechanics analysis of anisotropic plates by the boundary element method. *Int. J. Fract.* 64, 269–284.
- Watari, F., Yokoyama, A., Omori, M., Hirai, T., Kondo, H., Uo, M., Kawasaki, T., 2004. Biocompatibility of materials and development to functionally graded implant for bio-medical application. *Compos. Sci. Technol.* 64, 893–908.
- Woo, J., Meguid, S.A., Ong, L.S., 2006. Nonlinear free vibration behavior of functionally graded plates. *J. Sound Vib.* 289, 595–611.